IJASS
International Journal of
Aeronautical and Space Sciences

ORIGINAL PAPER

Check for updates

Rotorcraft Comprehensive Analysis Calculations of a Coaxial Rotor with Lift Offset

Jimmy C. Ho[1] · Hyeonsoo Yeo[2]

Abstract

This paper presents comparisons of rotor performance, blade pitch, rotor hub loads, and blade clearance between two sets of rotorcraft comprehensive analysis calculations and experimentally measured test data for a coaxial rotor system in forward flight conditions. The calculations are from the U.S. Army's Rotorcraft Comprehensive Analysis System (RCAS) with one set calculated using a prescribed vortex wake model and another set calculated by coupling RCAS to a viscous vortex particle method. For rotor performance and blade pitch, the calculations and test data are presented as functions of lift offset for four different advance ratios and for two different test upper rotor collective pitch settings. Rotor hub loads and blade clearance are compared on a time-varying basis for test points that form a lift offset sweep, an advance ratio sweep, and a rotor-to-rotor phase sweep. The main conclusion is that both sets of calculations generally reflect the same trends as the test data, which provides confidence in the ability of RCAS at calculating the aeromechanics behaviors of lift-offset coaxial rotors.

List of Symbols

A_{Ro}	Rotor disk area
A_{TS}	Test section area
C_D	Rotor drag coefficient
C_L	Rotor lift coefficient
C_Q	Rotor torque coefficient
C_T	Rotor thrust coefficient
c_d	Blade section drag coefficient
c_ℓ	Blade section lift coefficient
c_m	Blade section pitch moment coefficient
D	Rotor drag
D_e	Rotor effective drag
F_Z	Rotor hub vertical force
h_{res}	Flow field resolution parameter
L	Rotor lift
LO	Rotor lift offset
M	Mach number
M_X, M_Y	Rotor hub roll and pitch moment
Q	Rotor torque
R	Rotor radius
r	Blade radial position
V_∞	Freestream speed
α	Angle of attack
α_c	Corrected shaft angle
δ_W	Wall boundary correction factor
$\theta_0, \theta_{1c}, \theta_{1s}$	Rotor blade collective, lateral cyclic, and longitudinal cyclic pitch
μ	Rotor advance ratio
σ	Rotor solidity
ϕ	Rotor-to-rotor phase
ψ	Upper rotor azimuth
Ω	Rotor speed

Superscripts

L	Lower rotor
U	Upper rotor

✉ Jimmy C. Ho
    jimmy.c.ho2.ctr@mail.mil

[1] Science and Technology Corporation, Ames Research Center, Moffett Field, CA 94035, USA

[2] Aviation Development Directorate, U.S. Army Combat Capabilities Development Command Aviation & Missile Center, Ames Research Center, Moffett Field, CA 94035, USA

1 Introduction

Lift offset of a rotor is a measure of the ratio of its roll moment to its lift. As an edgewise rotor is subject to higher freestream speeds, the ability of its blades to produce lift on the advancing and retreating sides of the rotor disk increases and decreases, respectively. This asymmetry promotes a rotor roll moment (or lift offset) that increases with speed. However, conventional rotors are not structurally designed to

operate beyond low levels of roll moment. This limit on the allowable level of roll moment translates to a limit on the lift that may be generated on the advancing side, which leads to a reduction (relative to a rotor with no restrictions on roll moment) on the overall rotor lift available. The roll moment limit may also lead to lift distributions across the rotor disk that incur more power. Therefore, for high-speed aircraft with edgewise rotors, it is beneficial from an aerodynamic standpoint if the rotors are designed to operate with significant levels of lift offset.

The prevailing usage of edgewise rotors with lift offset is as the main rotors on helicopters featuring contra-rotating coaxial rotors. Sikorsky Aircraft has built and flown three such coaxial rotor helicopters thus far—the XH-59A [1], the X2 Technology™ Demonstrator [2], and the S-97 RAIDER® [3]. The XH-59A and X2 Technology™ Demonstrator are both flight demonstrators and have been retired while development of the S-97 RAIDER® remains ongoing. Another ongoing activity that utilizes the lift-offset coaxial rotor concept is the partnership between Sikorsky and Boeing to develop the SB>1 DEFIANT™ helicopter [4]. These continuing developments indicate a need to verify that computational tools are able to calculate the correct aeromechanics behaviors of lift-offset coaxial rotors. This verification may be accomplished by comparing calculations from the computational tools against experimentally measured test data.

A recent experiment by Cameron and Sirohi [5] provides useful test data for the purpose of verifying computational tools for lift-offset coaxial rotors in forward flight. The experiment includes testing in both coaxial and single rotor configurations. In the coaxial configuration, test conditions from these data form parametric variations in advance ratio and lift offset for different upper rotor collective pitch settings. There are also test conditions performed to study the effects of varying the rotor-to-rotor phase. The test data include measurements for individual rotor hub loads, individual blade pitch link force, blade clearance near the tip, and blade pitch angles. Rotor performance may be determined from the steady hub load measurements. Comparisons between calculations and this dataset exist for calculations using the rotorcraft comprehensive analysis tools UMARC [6,7] and CAMRAD II [8,9].

The goal of this paper is to present verification that the Rotorcraft Comprehensive Analysis System (RCAS; [10]) is able to correctly calculate the aeromechanics behaviors of lift-offset coaxial rotors by providing comparisons between RCAS calculations and the test data from Cameron and Sirohi [5]. Several refinements of the RCAS airloads and inflow models were implemented circa 2014 as documented by Saberi et al. [10] and Jain et al. [11]. These refinements enabled the successful validation of RCAS rotor aeromechanics calculations for single rotor [11–13], coaxial rotor [14,15], and tiltrotor [11,16,17] configurations. The validation for coaxial rotors [14,15] was limited to conditions in hover, so this paper aims to remedy the lack of RCAS validations for coaxial rotors in forward flight and with an emphasis on the effects of lift offset.

Two sets of RCAS calculations are presented in this paper. One set of calculations is performed using a prescribed vortex wake (PVW) inflow model. Another set of calculations is performed by coupling RCAS to the Advanced Rotorcraft Technology (ART) Inc.'s viscous vortex particle method (VVPM) tool that is described by He and Zhao [18,19]. For coaxial rotors, some validations [20] of VVPM exist in hover. RCAS v17.07.c6a and VVPM v3.0.0 are used for the calculations in this paper.

The next section describes the coaxial rotor tested by Cameron and Sirohi [5] and its testing. This is followed by a description of the analytical modeling used for both sets of RCAS calculations. Comparisons between RCAS calculations and test data are then shown. Rotor performance and blade pitch angles are shown as functions of lift offset at four different advance ratios. Although the focus here is on the coaxial rotor configuration, comparisons of rotor performance and blade pitch angles are also shown in the single rotor configuration. Detailed comparisons of rotor hub loads and blade clearance are then shown in the coaxial rotor configuration for specific test points that form a lift offset sweep, an advance ratio sweep, and a rotor-to-rotor phase sweep. Potential future work is then listed for readers who may be interested in seeking closer agreement between calculations and test data.

2 Rotor Description and Testing

Cameron and Sirohi [5] tested two-bladed hingeless rotors inside the Glenn L. Martin Wind Tunnel at the University of Maryland. The rotors were tested in the isolated lower rotor, isolated upper rotor, and coaxial rotor configurations. Testing in the isolated upper rotor configuration was performed in the presence of the lower rotor hub but with the lower blades removed, and vice versa for testing in the isolated lower rotor configuration. Figure 1 shows the experimental setup for the coaxial rotor configuration. The upper and lower rotors rotate counterclockwise and clockwise, respectively, if viewing the rotors from above. The rotor radius is 3.33 ft and the separation distance between the two rotors is $0.138R$. Each blade features a precone angle of $3°$. The blades are untwisted and untapered with a chord of 3.15 in, which yields a rotor solidity of 0.050 for a single rotor and 0.100 for the coaxial rotor system. A root reinforcement cuff, which extends from the blade root at $r = 0.12R$ to $0.35R$, is bonded to the blade to reduce blade flapping. The blade airfoil is a modified VR-12 except at locations inboard of $r = 0.35R$, where a fairing is used to cover the root reinforcement cuff. The airfoil is mod-
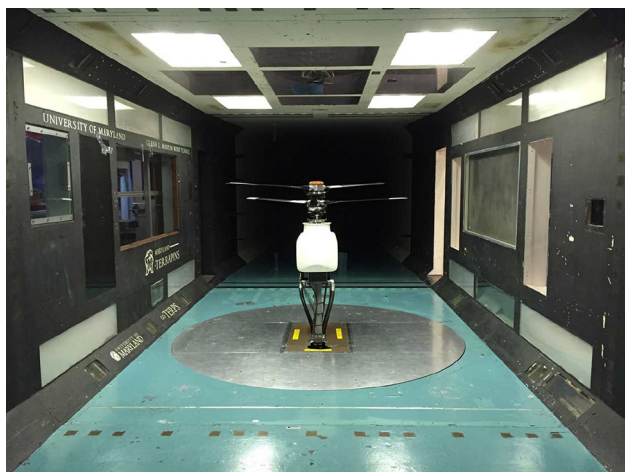
Fig. 1 Physical setup for testing the coaxial rotor

ified from the VR-12 by the addition of a trailing edge tab as shown by Schmaus and Chopra [6,7]. Differences exist in the blade pitch control arrangements (including different pitch link lengths, pitch link stiffnesses, and pitch horn lengths) between the two rotors, which lead to differences in pitch control stiffness. Cameron [21] provides more details, including blade properties, of the rotors for interested readers.

Test data were collected for 177, 169, and 362 test points in the isolated lower, isolated upper, and coaxial rotor configuration, respectively. The nominal baseline rotor speed is 900 RPM. The wind tunnel airspeed was adjusted to achieve target advance ratios of 0.2, 0.3, 0.4, and 0.5. Target values for lift offset were 0, 0.05, 0.10, 0.15, and 0.20. Testing in the isolated rotor configuration was performed by setting the rotor collective pitch and then adjusting the two cyclic pitch angles to achieve zero pitch moment and the roll moment required for the desired lift offset. Collective pitch settings tested in the isolated rotor configuration included 2°, 3°, 4°, 6°, 8°, and 10°. The blade pitch angle sensors are stated to be accurate within ± 0.5° [5]. Testing in the coaxial rotor configuration was performed by setting the upper rotor collective pitch and then adjusting the remaining five pitch controls (θ_0^L, θ_{1c}^U, θ_{1s}^U, θ_{1c}^L, and θ_{1s}^L) to achieve system torque balance, zero individual rotor pitch moment, and the individual rotor roll moment for the desired coaxial system lift offset. Upper rotor collective pitch settings tested in the coaxial rotor configuration included 2°, 4°, 6°, and 8°. While most test points in the coaxial rotor configuration were tested with zero rotor-to-rotor phase, some were tested with this phase set to 20° or 45°. Likewise, while most test points in the coaxial configuration were tested at a rotor speed of 900 RPM, some were tested at 1200 RPM.

Lift offset and rotor performance are determined from steady values of the rotor hub loads. Lift offset is defined here as

$$LO = \frac{M_X}{RL} \quad \text{for a single rotor}$$

$$LO = \frac{M_X^U + M_X^L}{R\left(L^U + L^L\right)} \quad \text{for a coaxial system .} \tag{1}$$

In the above definition, rotor roll moment is defined positive towards the retreating side, and rotor lift is perpendicular to the freestream velocity and positive up. A popular parameter for evaluating forward flight efficiency of a rotor is its lift-to-effective-drag ratio. This parameter is defined as

$$L/D_e = \frac{V_\infty L}{\Omega Q + V_\infty D} \quad \text{for a single rotor}$$

$$L/D_e = \frac{V_\infty\left(L^U + L^L\right)}{\Omega\left(Q^U + Q^L\right) + V_\infty\left(D^U + D^L\right)} \tag{2}$$

for a coaxial system.

In the above definition, rotor torque is positive if it opposes the rotational direction, and rotor drag is positive along the freestream direction. The terms ΩQ and $V_\infty D$ are referred to as the shaft power and drag power, respectively. The denominator in the above expression is the sum of these two powers. For this experiment, the distinction between rotor thrust and lift is negligible since the shaft is set perpendicular to the freestream velocity.

Load cells were used to measure hub forces and moments in all three directions for both rotors. Tension–compression load cells were used to measure pitch link force for all blades. An optical sensor was placed at the lower surface of one of the upper rotor blades around $r = 0.9R$ to measure its clearance with lower rotor blades during blade crossings. Linear Hall effect sensors were used to measure blade pitch angles at the blade root. For test points with rotor speeds of 900 and 1200 RPM, data were collected at 2000 and 1500 azimuthal locations per revolution, respectively. For each test point, the test data presented here are phase-averaged over 100 consecutive rotor revolutions of data and with the 36th harmonic contents removed (to remove potential noise that would be introduced by a 36-toothed drive pulley that was used to ensure synchronization between the two rotors).

3 Analytical Modeling

3.1 Dynamic System

A common elastic multibody dynamics model is used for performing RCAS calculations by the PVW inflow model as well as coupling with VVPM. For the coaxial configuration, the two rotors are connected by a massless rigid bar that represents the shaft connection. For both coaxial and single rotor configurations, the rotor system is treated as being in
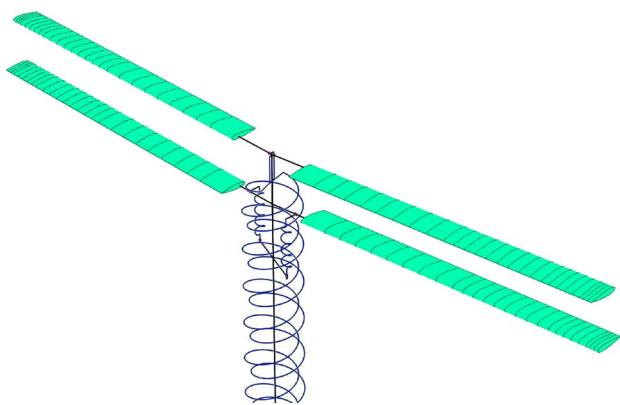
Fig. 2 RCAS model of the coaxial rotor

Table 1 Non-rotating blade frequencies without pitch links

Mode	Test	RCAS
First flap (Hz)	16.2	15.8
First lag (Hz)	65.0	75.6
Second flap (Hz)	92.1	89.8
First torsion (Hz)	159.7	155.4

Fig. 3 Calculated blade frequencies in vacuo with zero blade pitch

isolation so that the customary approximations of neglecting effects from the dynamics of the engine, drive train, and test stand are applied. For each blade, pertinent modeling features include a pitch bearing, rigid bars and a translational spring to represent the pitch control linkages and its flexibility, a slide element for blade pitch control inputs, and 9 nonlinear beam elements to model elastic deformations of the blade. The beam elements are numerical implementations of the Hodges–Dowell [22] nonlinear beam theory. To allow for large elastic deformations, the deformations within each nonlinear beam element are calculated in its own element frame that is located at the root node of the element. Following the assumption of Schmaus and Chopra [6,7] in building their UMARC model, the blade modes include a structural damping value of 2%. Figure 2 is a graphical depiction of the RCAS coaxial rotor model and is shown here for the purpose of providing readers with an overall sense of the modeling. All calculations are performed using 72 azimuthal steps per revolution.

The wind tunnel walls are not modeled, so the shaft angles used in the analyses are corrected to reflect wall induced interference effects. These wall corrections are calculated based on the Glauert methodology [23] using the following formula:

$$\alpha_c = \frac{2\delta_W C_T A_{Ro}}{\mu^2 A_{TS}}. \tag{3}$$

For the current problem, Fig. 10.17 of Barlow et al. [24] approximates δ_W to be 0.152, A_{Ro} is 34.9 ft^2 (disk area of a single rotor even in the coaxial configuration), and A_{TS} is 85.1 ft^2 (rectangular 7.74-by-10.99 ft test section). The sign of δ_W is positive from having a closed test section and leads to positive values for α_c, which implies backwards shaft tilt.

With one blade aligned vertically and clamped at its root end (see Fig. 4.24 from Cameron [21]), the blade was excited by an electrodynamic shaker to measure its non-rotating frequencies. The hub and pitch links were absent during this testing (and the blade precone is also eliminated), so the measured torsion frequency is not representative of a blade with its pitch links attached. Table 1 lists the measured frequencies of the first four modes with its corresponding RCAS calculations for a blade in this configuration. The RCAS calculations are reasonably close to the test data except for the lag mode. Yeo et al. [25] showed that RCAS frequency calculations for beam-like structures are accurate, so the discrepancies with test data here are likely due to a lack of accuracy in beam properties.
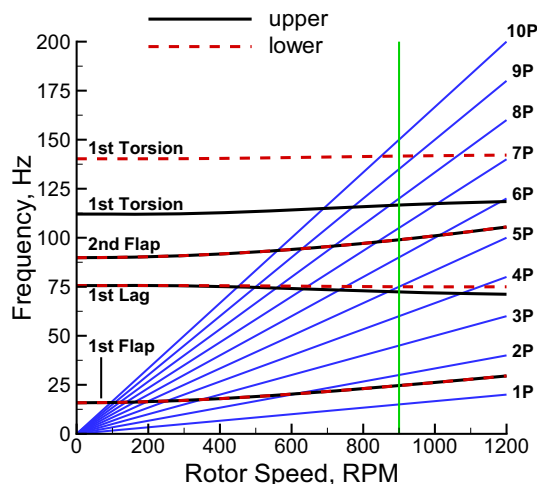
Figure 3 shows RCAS calculations of the blade modal frequencies in vacuo with zero blade pitch as functions of rotor speed up to 1200 RPM (the highest speed tested) for both the upper and lower rotors. The aforementioned differences in pitch control stiffness between the two rotors manifest itself here with torsion frequency of the upper rotor blades being much lower than that of the lower rotor blades. A vertical line is drawn to highlight frequencies at 900 RPM, which is the rotor speed of the test points examined in this paper. Starting from the lowest frequency mode, the modes are characterized as first flap, first lag, second flap, and first torsion. Straight lines are drawn to indicate frequencies that are integer multiples of the rotor speed (e. g., "2P" represents the product of the number two and the rotor speed). There are ample frequency separations between the modes, so interactions between them are not expected. The blade pitch/torsion

content increases in the first lag mode with increasing rotor speed, which results in the decrease in frequency of this mode as rotor speed increases. The increase in the pitch/torsion content of this mode arises from both the blade precone and the flexibility of the pitch control linkages. At 900 RPM, the first four frequencies are 1.6, 4.8, 6.6, and 7.8 per rev for the upper rotor blades. Typical of rotors designed to operate with significant lift offset, the flap and lag frequencies are much greater than those of conventional helicopter rotors. Note that with the pitch links attached, the non-rotating torsion frequency has been lowered from 155.4 Hz to 112.1 and 140.3 Hz for the upper and lower rotor blades, respectively.

There are distinctions between this RCAS model and the aforementioned UMARC [6,7] and CAMRAD II [8,9] models—one related to pitch bearing damping and the other to blade flapping. Both the UMARC and the CAMRAD II models include damping in the blade pitch bearing. For both models, the damping constant was adjusted so that pitch link force calculations would match well with the test data. Considering that those two models employ different levels of damping (0.0074 lb ft s/rad for UMARC and 0.0221 lb ft s/rad for CAMRAD II), the current authors choose not to model pitch bearing damping and choose not to compare pitch link force between RCAS calculations and test data. While pitch link force should affect blade torsion moment calculations, its influence should be negligible for the quantities that are shown in this paper (especially since Fig. 3 shows no coupling between torsion and the other modes). For the distinction related to blade flapping, the CAMRAD II model was modified so that its calculated blade clearance would decrease to match the measured value for one particular test point. Feil et al. [9] achieved this goal for the CAMRAD II model by adjusting the flap bending stiffness at the blade root. However, the CAMRAD II calculations for blade clearance only match the test data well for limited test conditions even with the adjustment. Due to this limited success, the current authors choose not to alter the blade flapping characteristics of their RCAS model.

3.2 Trim

The blade collective, lateral cyclic, and longitudinal cyclic pitch angles for each rotor are determined from a trim analysis. RCAS calculations in the isolated rotor configuration are performed to compare rotor performance and blade pitch angles with test data. In this configuration, the three angles (or trim variables) are adjusted to match the measured lift (from a least squares fit of the test data), zero pitch moment, and the roll moment required to achieve the desired lift offset (i. e., $M_X = LO(RL)$). RCAS calculations in the coaxial rotor configuration are performed to compare rotor performance, blade pitch angles, and time-varying quantities (hub loads and blade clearance) with test data. For rotor

performance calculations, the six blade pitch angles (three from each rotor) are adjusted to match the measured system lift (from a least squares fit of the test data), system torque balance, zero pitch moment for each rotor, and the roll moment required to achieve the desired lift offset for each rotor (while satisfying roll moment balance so that $M_X^U = M_X^L = LO(R)(L^U + L^L)/2$). For calculations of time-varying quantities, which are compared with test data for specific test points, the same trim targets are used except that the measured system lift is taken from its value corresponding to each test point.

Distinctions exist in the described trim analysis from the aforementioned works using UMARC [6,7] and CAMRAD II [8,9]. In the isolated rotor configuration, both the UMARC and CAMRAD II calculations were performed by setting the collective pitch to its test value and then adjusting its two cyclic pitch angles to satisfy zero pitch moment and the desired roll moment. While this is how the physical experiment was conducted, the calculated rotor lift values do not match the measured lift. For rotor performance calculations in the coaxial configuration, both the UMARC and CAMRAD II calculations were performed by setting the upper rotor collective pitch to its test value and then adjusting its remaining five pitch angles (θ_0^L, θ_{1c}^U, θ_{1s}^U, θ_{1c}^L, and θ_{1s}^L) to achieve system torque balance and the desired individual rotor pitch and roll moments. The calculated rotor lift (both individual and system lift) again does not match the measured lift. For calculations of time-varying quantities in the coaxial configuration, the CAMRAD II calculations were performed in this same way. The UMARC calculations were instead calculated by adjusting all six blade pitch angles to achieve the measured individual rotor lift, pitch moment, and roll moment; this implies that the system torque was not balanced.

3.3 RCAS PVW Analysis

In regard to the RCAS vortex wake model, the rotor blades are modeled as lifting lines with bound vortices located along the blade quarter chord. For each blade, the lifting line encompasses the inboard end of the root fairing to the blade tip. Each lifting line is discretized into a series of 26 spanwise aerodynamic segments, or "aerosegments." The wake behind the blade is comprised of vortices trailing from the edge of each of the aerosegments. Shed vortices are also included to model the effects of azimuthally varying blade circulation distribution. An azimuthal region behind the blade called the "near-wake" includes all of these individual vortices over the entire blade span. At the termination of this near-wake region, a simpler "far-wake" model is used. The far-wake is comprised of a discrete tip vortex and a large-core vortex representing the inboard wake sheet trailing from the entire blade span. The tip vortex core size is set to be 20%

of the blade chord. The extent of the near-wake and far-wake is set to wake ages of 60° and 6 revolutions, respectively. While RCAS has the option of using a free vortex wake (FVW) model to calculate the force-free convection of the tip vortex, it is not used given that the lowest advance ratio examined here is 0.2. At such high advance ratios, the tip vortices convect away from the rotors at such a high rate that effects from allowing the tip vortices to deform are negligible. With the exception of not using the FVW model, the described vortex wake model is consistent with what was used for RCAS calculations of helicopter rotor performance [11] and blade loads [12] in forward flight. The RCAS PVW calculations here are performed using 72 azimuthal steps per revolution.

The aerodynamic interference between the two rotors is calculated directly using the vortex wake models. In other words, the induced velocity felt by one rotor includes the induced velocity that is calculated from the vortices of the other rotor in addition to its own self-induced vortices.

Airloads are calculated for each aerosegment. Sectional lift, drag, and pitch moment along the blade are determined from airfoil lookup tables with corrections for yawed flow effects. The airfoil tables contain values of c_ℓ, c_d, and c_m as functions of α and M. Not having airfoil tables for the root fairing, the VR-12 tables are used for all aerosegments. Note that the VR-12 tables used for this work came from Sikorsky while the tables used in the UMARC [6,7] and CAMRAD II [8,9] analyses were calculated using the computational fluid dynamics (CFD) tool TURNS [26]. In addition to the yawed flow corrections, the airloads calculations include an implementation of the linear unsteady airloads model by Theodorsen [27] and Greenberg [28].

3.4 Coupled RCAS–VVPM Analysis

The differences between the RCAS PVW analysis and the coupled RCAS–VVPM analysis are from induced velocity calculations (which has an influence on the rest of the aeroelastic system). In both analyses, the airloads—the calculations of which are directly dependent on induced velocity—and trim calculations are performed by RCAS as described in the previous subsections. The coupling procedure between RCAS and VVPM is an iterative loose-coupling that is conceptually equivalent to the "wake coupling" described by Wachspress et al. [29,30]. For each blade, 26 aerosegments are used again for the RCAS airloads calculations as using more only resulted in negligible changes. Unlike coupling to a CFD tool (which is computationally expensive), the computational time required for performing coupled RCAS–VVPM analyses is actually less than it takes for RCAS PVW analyses (although it should be pointed out that coupled RCAS–VVPM analyses require usage of a graphics processing unit, whereas standalone RCAS analyses merely use a single-core central processing unit). The coupled RCAS–VVPM calculations here are performed using 72 azimuthal steps per revolution for both computational tools.

VVPM solves the velocity–vorticity form of the incompressible Navier–Stokes equations for an accurate solution of the rotor wake [18,19]. It is especially attractive for its lack of empirically based parameters (e. g., wake parameters from vortex wake models). Upon given the blade motion and blade-bound circulation from RCAS, VVPM generates vortex particles that originate from the blade lifting line and are convected into the wake. The trajectory of each particle is based on its velocity, which is the resultant of freestream velocity and induced velocity from all vortex particles (including those from another rotor). The only user-input parameter in VVPM is the flow field resolution parameter h_{res}. It defines the initial discretization of the vortex particles emanating from the blade bound circulation. The value of this parameter, which is nondimensionalized by R, is set to $h_{res} = 0.05$ for the calculations in this paper.

4 Rotor Performance and Trim

4.1 Isolated Lower Rotor

This subsection compares rotor performance and trim variables (i. e., blade pitch angles) between the RCAS PVW calculations and test data in the isolated lower rotor configuration. The coupled RCAS–VVPM calculations are not shown here to reduce repetition and since they do not differ greatly from the RCAS PVW calculations.

The calculated rotor lift, lift-to-effective-drag ratio, sum of shaft and drag power, shaft power, drag power, collective pitch, lateral cyclic pitch, and longitudinal cyclic pitch are compared against the measured values in Fig. 4 as functions of advance ratio for zero lift offset and test collective pitch settings of $\theta_0 = 3°$, $5°$, $8°$, and $10°$. Test points plotted are the ones that are both within 0.25° of the stated collective pitch and within 0.04 of $LO = 0$. The calculated lift match the test data since lift is one of the trim targets, which also implies that differences between calculations and test data for L/D_e are entirely due to differences in the sum of shaft and drag power. The agreement between calculations and test data is good for L/D_e at low collectives ($\theta_0 = 3°$ and $5°$), but the calculations are much higher than the test data at higher collectives ($\theta_0 = 8°$ and $10°$). At these higher collectives, the reason for the higher calculated L/D_e is that the calculations are much lower than test data for shaft power. This difference in shaft power increases as θ_0 increases. Note that, at these higher collectives, the measured shaft power is highly nonlinear with respect to θ_0, which is unusual given that the rotor should not be operating in stall at $\theta_0 \leq 10°$. As with performance parameters, the agreement between calculations and test data
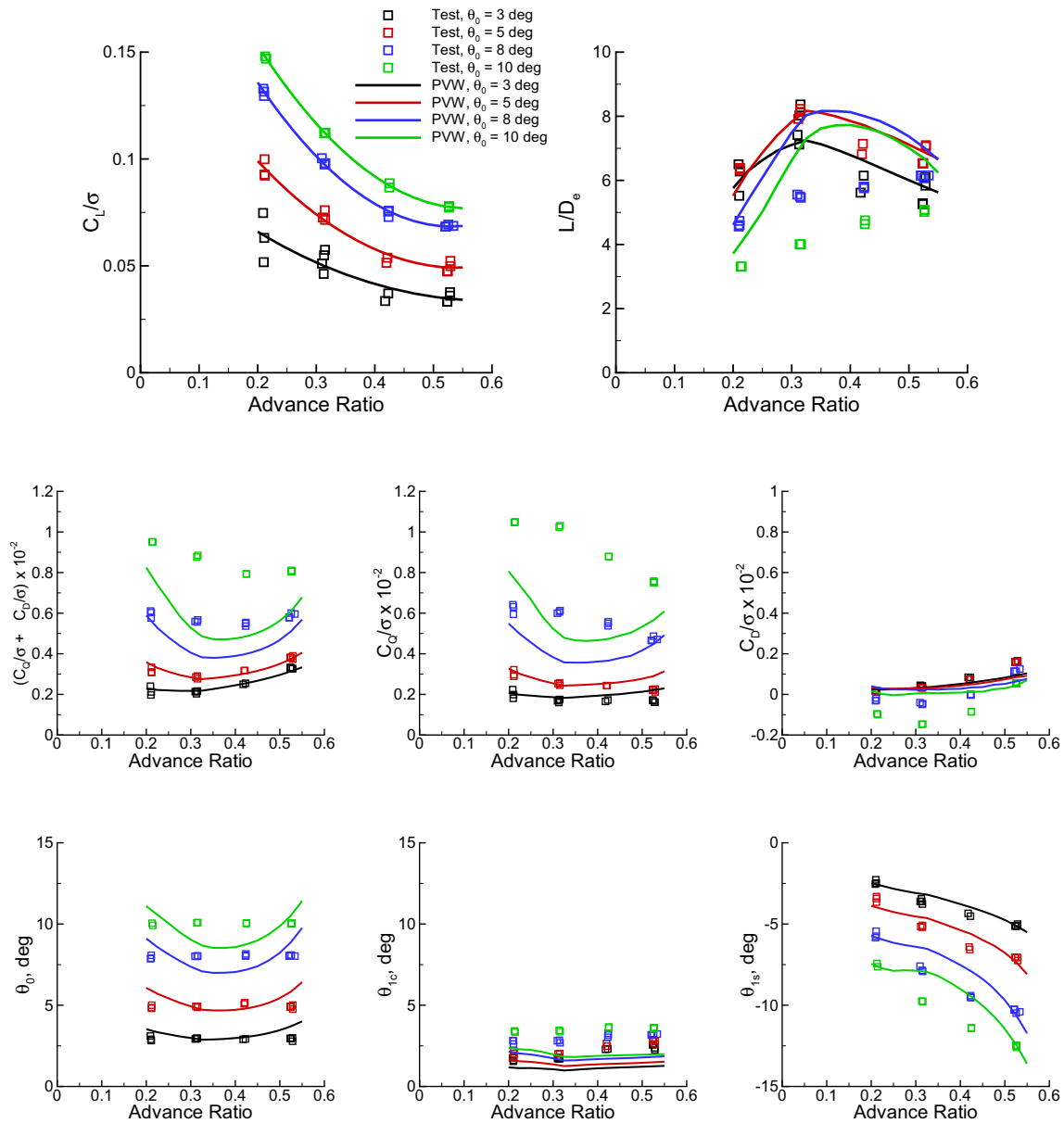
Fig. 4 Rotor parameters as functions of advance ratio in the isolated lower rotor configuration for zero lift offset and various test collective pitch settings. Comparison between RCAS PVW calculations and test data

for blade pitch angles is good at low collectives and worsens with increasing θ_0.

Figures 5 and 6 show the same performance parameters and blade pitch angles as functions of lift offset for test collective pitch settings of $\theta_0 = 3°$ and $8°$, respectively. Each figure contains data for advance ratios of $\mu = 0.21, 0.31, 0.42$, and 0.53. Test points plotted are within $0.25°$ of the stated collective pitch. The calculations and test data are in good agreement for L/D_e (and hence the sum of shaft and drag power) for a test collective of $\theta_0 = 3°$, but the calculated L/D_e are generally higher for a test collective of $\theta_0 = 8°$ due to calculating lower values of shaft power; these trends

are consistent with what is shown for zero lift offset from Fig. 4. For the test collective of $\theta_0 = 3°$, the calculations and data are in good agreement for both shaft and drag power at $\mu = 0.21$ and 0.31. However, at $\mu = 0.42$ and 0.53, the calculations show higher shaft power and lower drag power that result in fortuitously good agreement with test data in the sum of shaft and drag power. In Fig. 6, "Adjusted L/D_e" values are shown in which the calculated L/D_e curves are shifted vertically down by 0.2, 1.6, 2.2, and 0.9 for $\mu = 0.21, 0.31, 0.42$, and 0.53, respectively. With the exception of $\mu = 0.31$, these adjusted L/D_e values are in good agreement with the measured values and illustrate that RCAS is at least accurate at
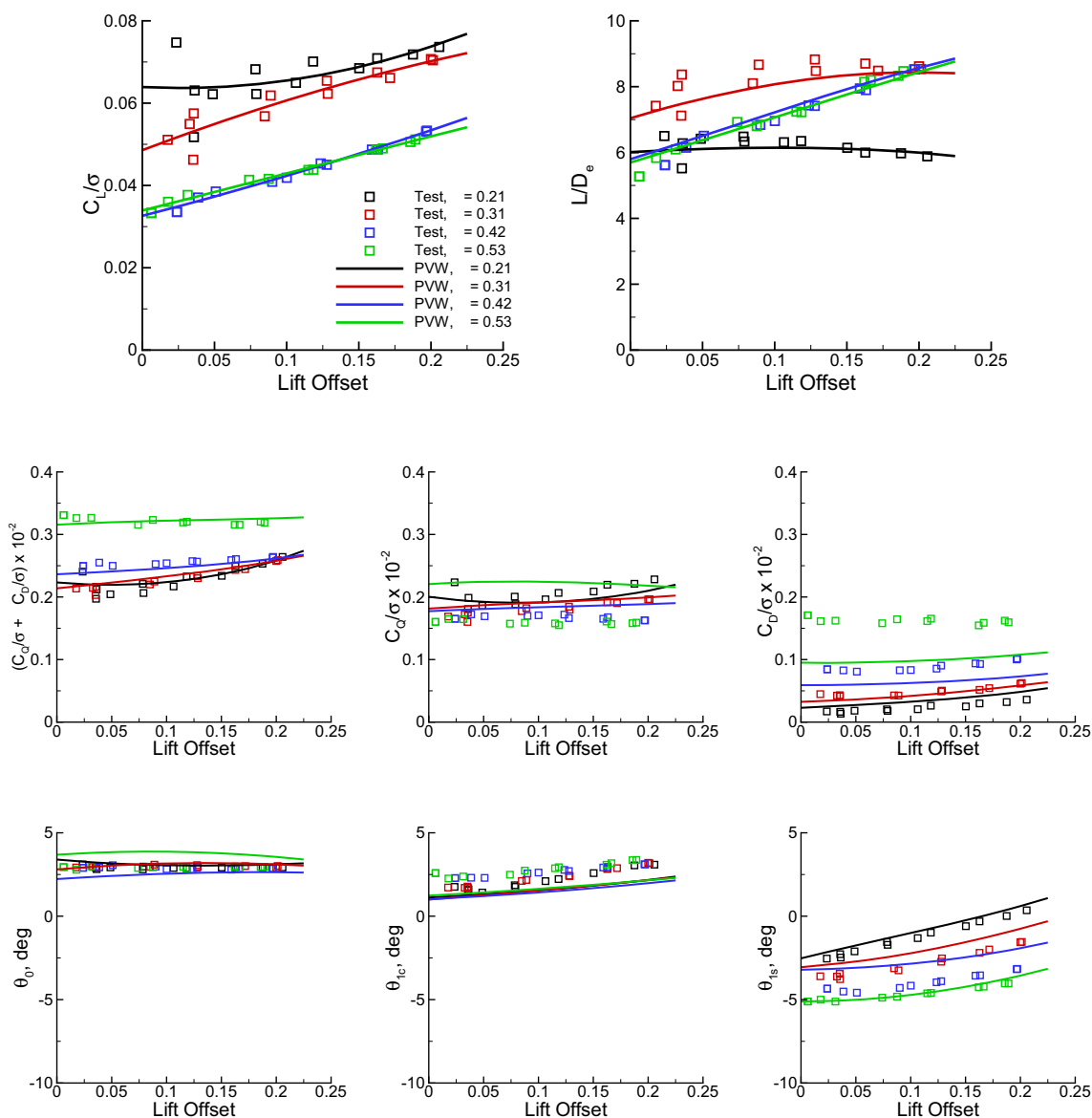
Fig. 5 Rotor parameters as functions of lift offset in the isolated lower rotor configuration for a test collective pitch setting of 3° and various advance ratios. Comparison between RCAS PVW calculations and test data

calculating the change in L/D_e with respect to lift offset. For both test $\theta_0 = 3°$ and $8°$, the RCAS calculations for the collective and cyclic pitch angles show the same trends with lift offset as the test data although constant offsets do exist in some of these comparisons.

Using L/D_e as the measure for efficiency, Figs. 5 and 6 both show that the benefits of lift offset increases with increasing advance ratio. For $\mu = 0.21$, the L/D_e curve is mostly flat at low lift offsets ($LO < 0.1$) and decreases for higher lift offsets. For $\mu = 0.31$, the L/D_e curve increases at low lift offsets before becoming flat at higher lift offsets. For both $\mu = 0.42$ and 0.53, the L/D_e curve increases with increasing lift offset for the entire range examined. Note that while lift offset should be beneficial for rotor efficiency (espe-

cially with increasing advance ratio), readers should be aware that the results here are distorted in that they artificially favor increasing lift offset. The reason for this is that rotor lift is not kept constant with increasing lift offset and is discussed more at the end of the ensuing subsection.

4.2 Coaxial Rotor

Rotor performance and trim variables are examined here in the coaxial rotor configuration. Calculations include those from both the RCAS PVW and coupled RCAS–VVPM analyses.

Figures 7 and 8 show a comparison between RCAS PVW calculations and test data for both individual rotor and system
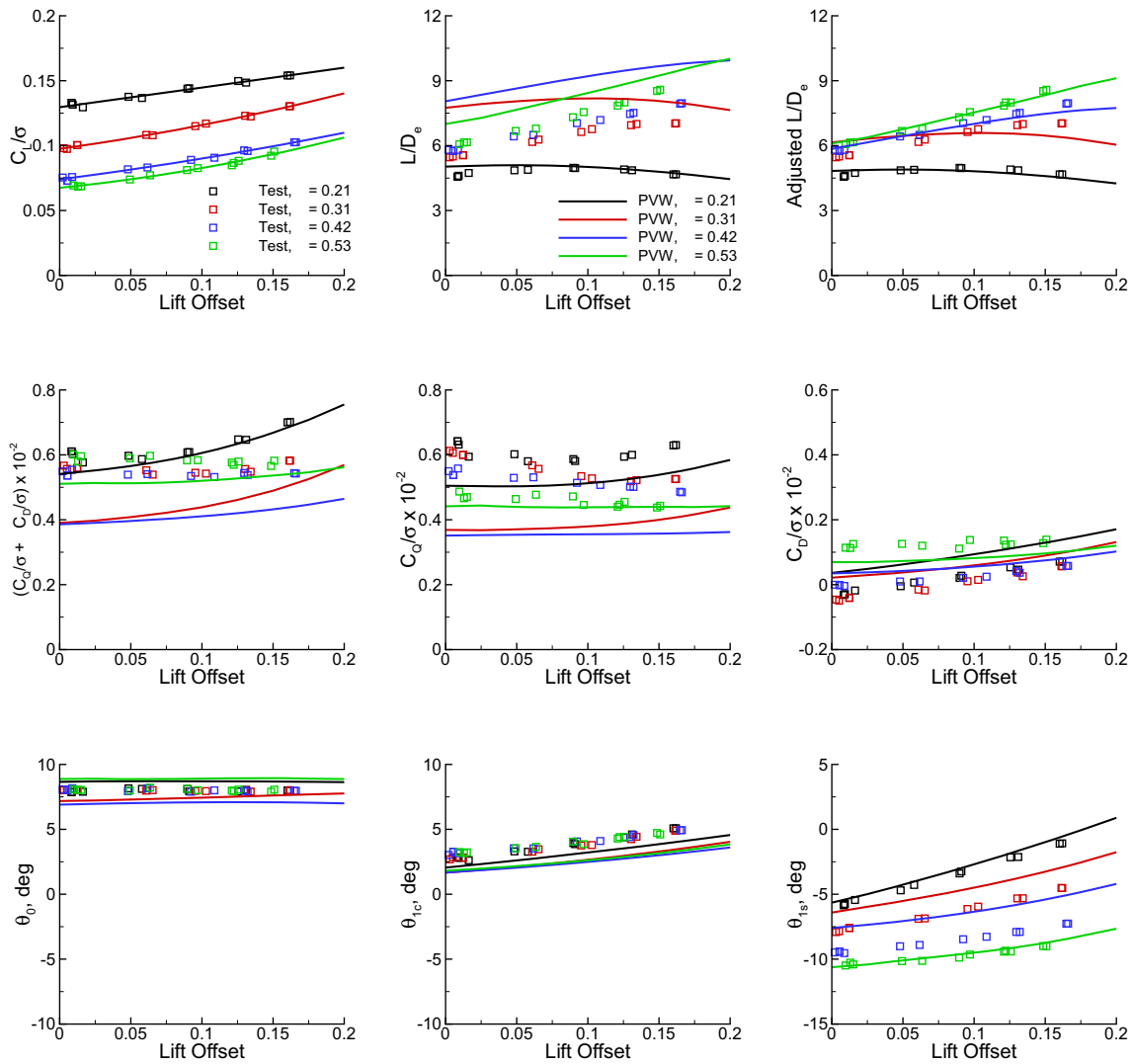
Fig. 6 Rotor parameters as functions of lift offset in the isolated lower rotor configuration for a test collective pitch setting of 8° and various advance ratios. Comparison between RCAS PVW calculations and test data

parameters as functions of system lift offset for test upper rotor collective pitch settings of $\theta_0^U = 2°$ and 8°, respectively. The individual rotor parameters examined here are the same ones from the previous subsection. The system parameter examined here is the lift-to-effective-drag ratio. Each figure contains data for advance ratios of μ of approximately 0.21, 0.31, 0.42, and 0.53. Test points plotted are within 0.25° of the stated upper rotor collective pitch. For a torque-balanced ($C_Q^U = C_Q^L$) coaxial rotor system in hover, it is known that the upper rotor produces more lift than the lower rotor [14]. In contrast to hover, the test data here consistently show that the lower rotor produces more lift. The calculations also show this phenomenon except for the cases of test $\theta_0^U = 2°$ and $\mu = 0.21$. The calculations generally show a much different lift sharing (between the two rotors) from the test data for the test $\theta_0^U = 2°$ cases, but it resembles the test data for the test

$\theta_0^U = 8°$ cases. For the test $\theta_0^U = 2°$ cases, the difference in power (in both shaft and drag power) between calculations and test data is small at $\mu = 0.21$ and 0.31, but this difference in power grows with increasing advance ratio and results in a similarly growing difference in system L/D_e. For the test $\theta_0^U = 8°$ cases, the calculations show much lower levels of shaft power than the test data (which is consistent with the isolated rotor results for $\theta_0 = 8°$) and result in higher values for both individual and system L/D_e. Adjusted L/D_e values are shown by vertically shifting each of the calculated system L/D_e curves down. For the test $\theta_0^U = 2°$ cases, the vertical shift is 0.2, 0.4, 0.7, and 0.7 for $\mu = 0.21$, 0.31, 0.42, and 0.53, respectively. For the test $\theta_0^U = 8°$ cases, the vertical shift is 0.5, 1.8, 2.1, and 1.7 for $\mu = 0.21$, 0.32, 0.43, and 0.53, respectively. The adjusted system L/D_e values are in good agreement with the measured values and illustrate
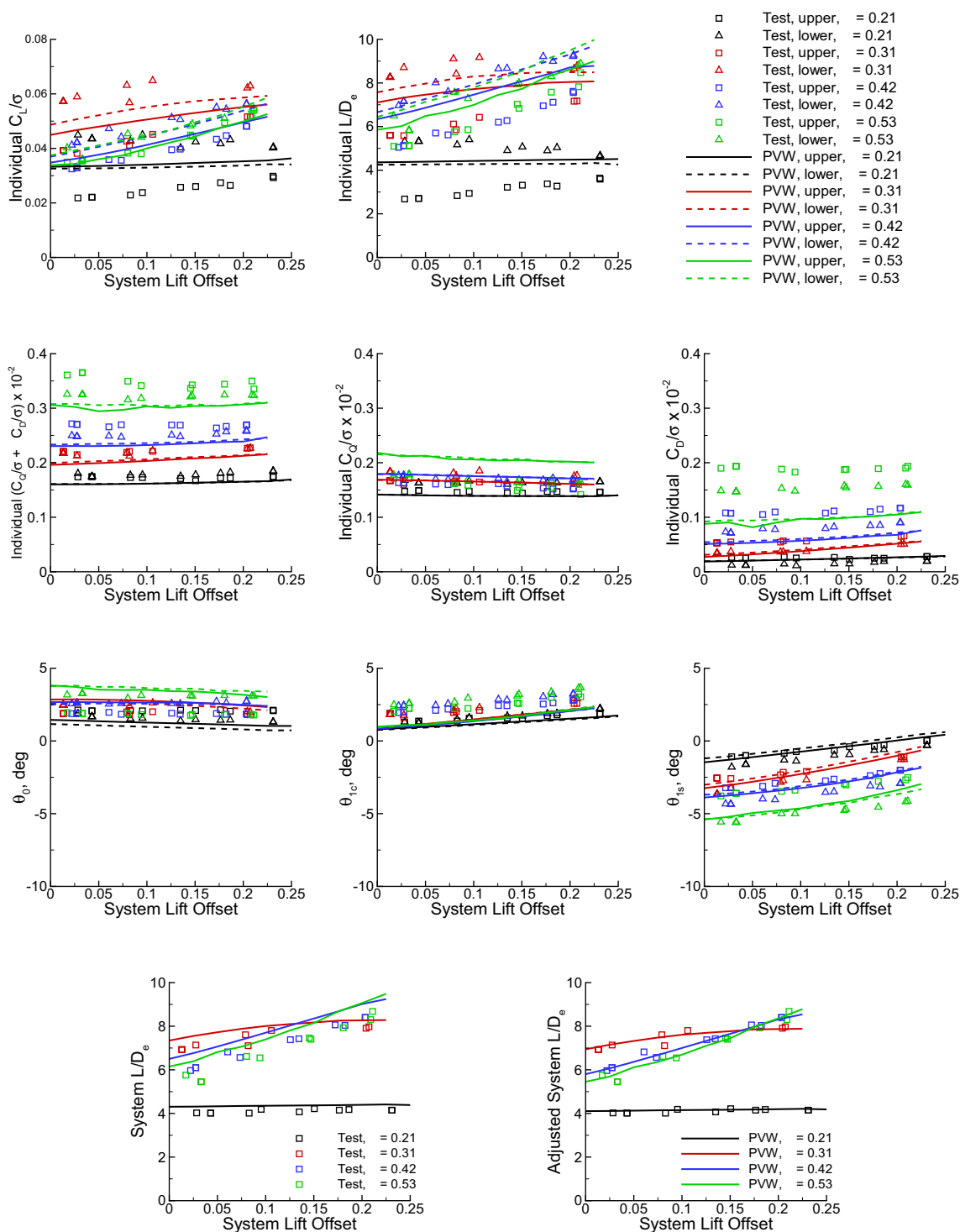
Fig. 7 Rotor parameters as functions of system lift offset in the coaxial rotor configuration for a test upper collective pitch setting of 2° and various advance ratios. Comparison between RCAS PVW calculations and test data

that the RCAS PVW calculations are accurate at calculating changes in system L/D_e with respect to lift offset. As with the isolated rotor results, the calculations for all collective and cyclic pitch angles show the same trends with lift offset as the test data although constant offsets do exist.

The comparison between the coupled RCAS–VVPM calculations and test data for the same parameters are shown in Figs. 9 and 10 for test upper rotor collective pitch settings of $\theta_0^U = 2°$ and 8°, respectively. The calculated lift sharing is often different between RCAS–VVPM and RCAS PVW
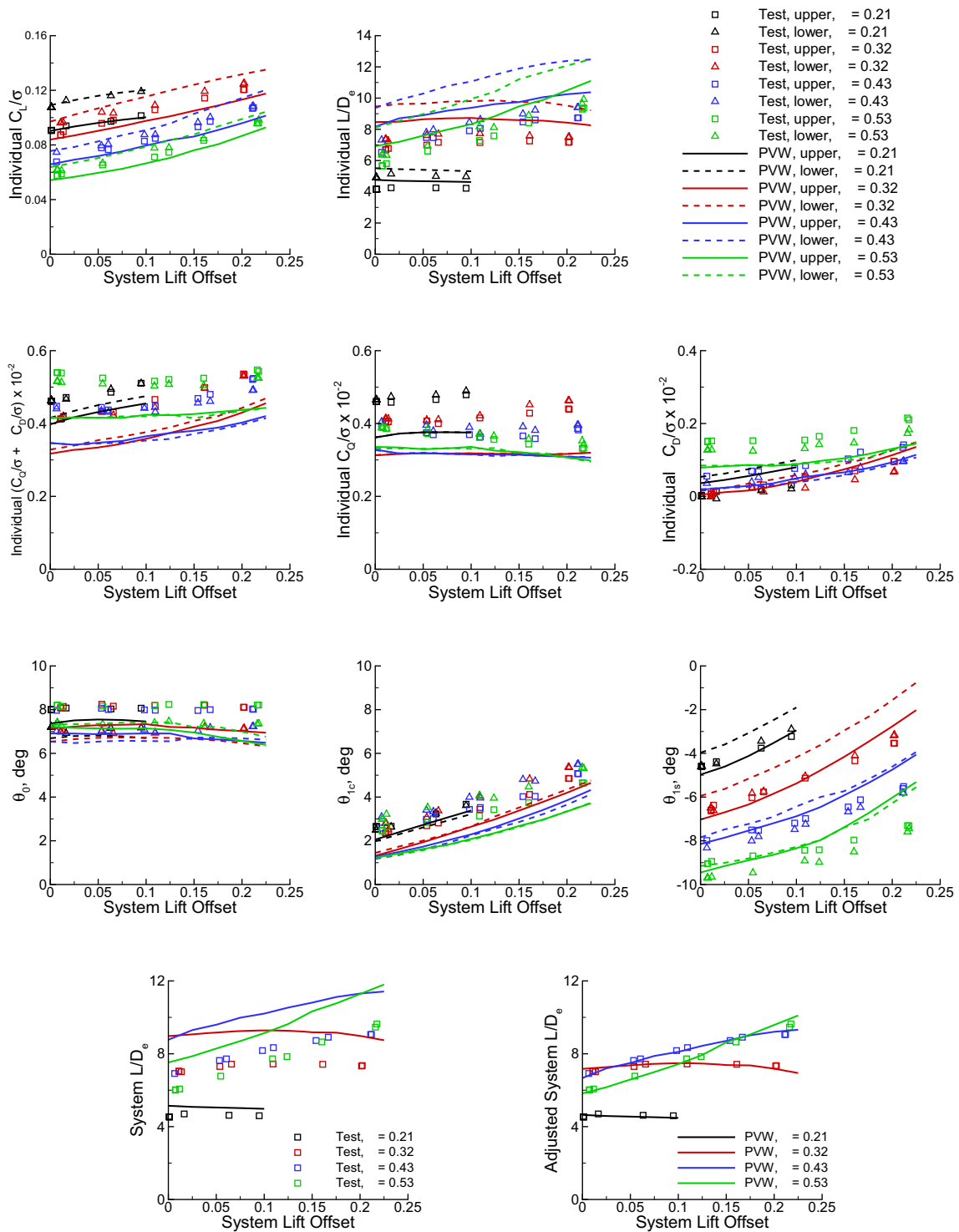
Fig. 8 Rotor parameters as functions of system lift offset in the coaxial rotor configuration for a test upper collective pitch setting of 8° and various advance ratios. Comparison between RCAS PVW calculations and test data

with the RCAS–VVPM calculations showing much better agreement with test data in certain cases (most notably for the cases of test $\theta_0^U = 2°$ and $\mu = 0.21$). Although significant differences in power and L/D_e exist between the two sets of

calculations, the trends regarding how they compare with test data are the same. For the test $\theta_0^U = 2°$ cases, the adjusted system L/D_e values are shifted vertically down from the calculated values by 0.35, 0.1, 0.4, and 0.85 for $\mu = 0.21$,
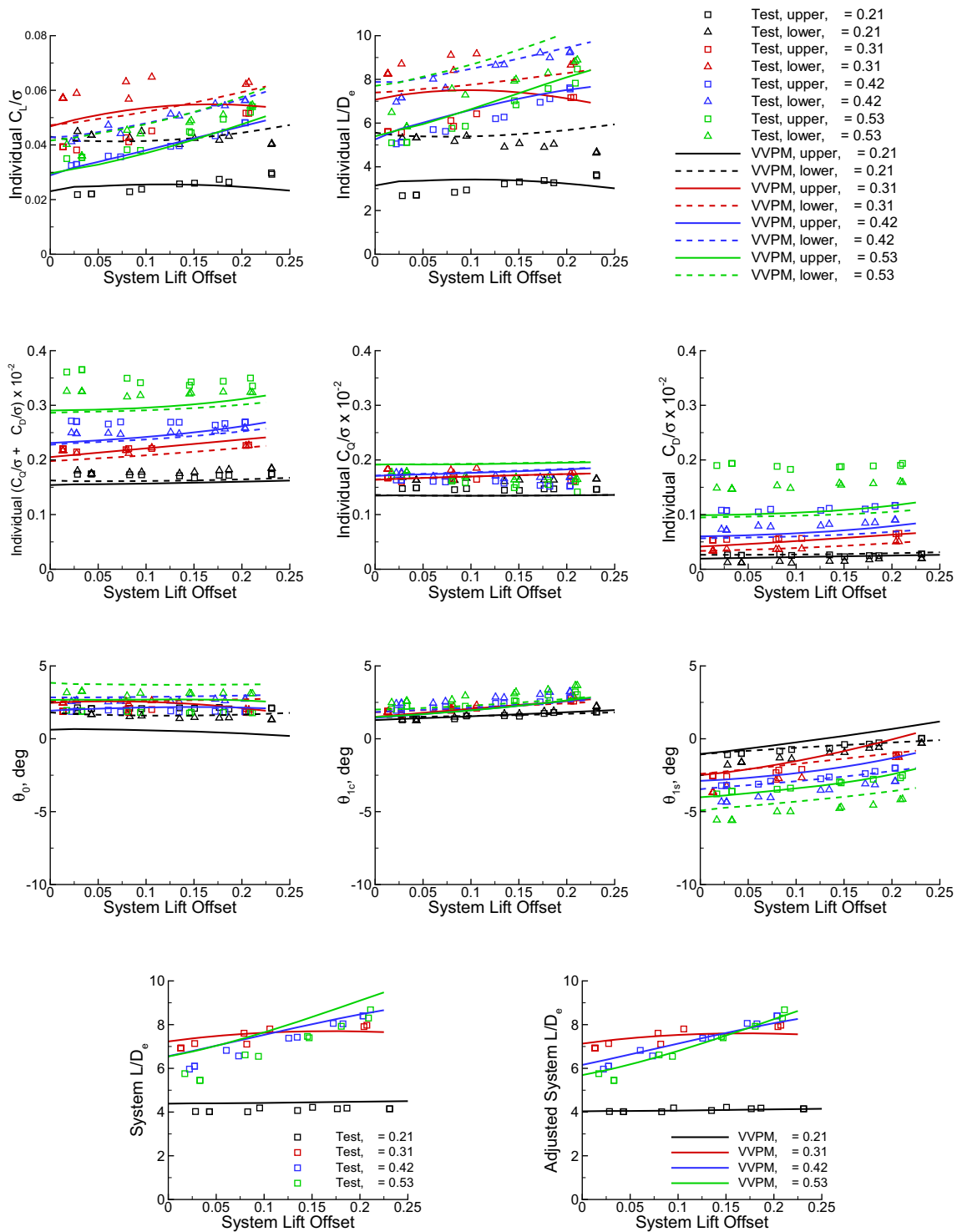
Fig. 9 Rotor parameters as functions of system lift offset in the coaxial rotor configuration for a test upper collective pitch setting of 2° and various advance ratios. Comparison between coupled RCAS–VVPM calculations and test data

0.31, 0.42, and 0.53, respectively. For the test $\theta_0^U = 8°$ cases, the vertical shift is 0.4, 1.3, 1.8, and 2.7 for $\mu = 0.21$, 0.32, 0.43, and 0.53, respectively. Other than the cases of test $\theta_0^U = 8°$ and $\mu = 0.32$, the adjusted system L/D_e values are

in good agreement with the measured values. The RCAS–VVPM calculations for the collective and cyclic pitch angles usually show the same trends with lift offset as the test data,
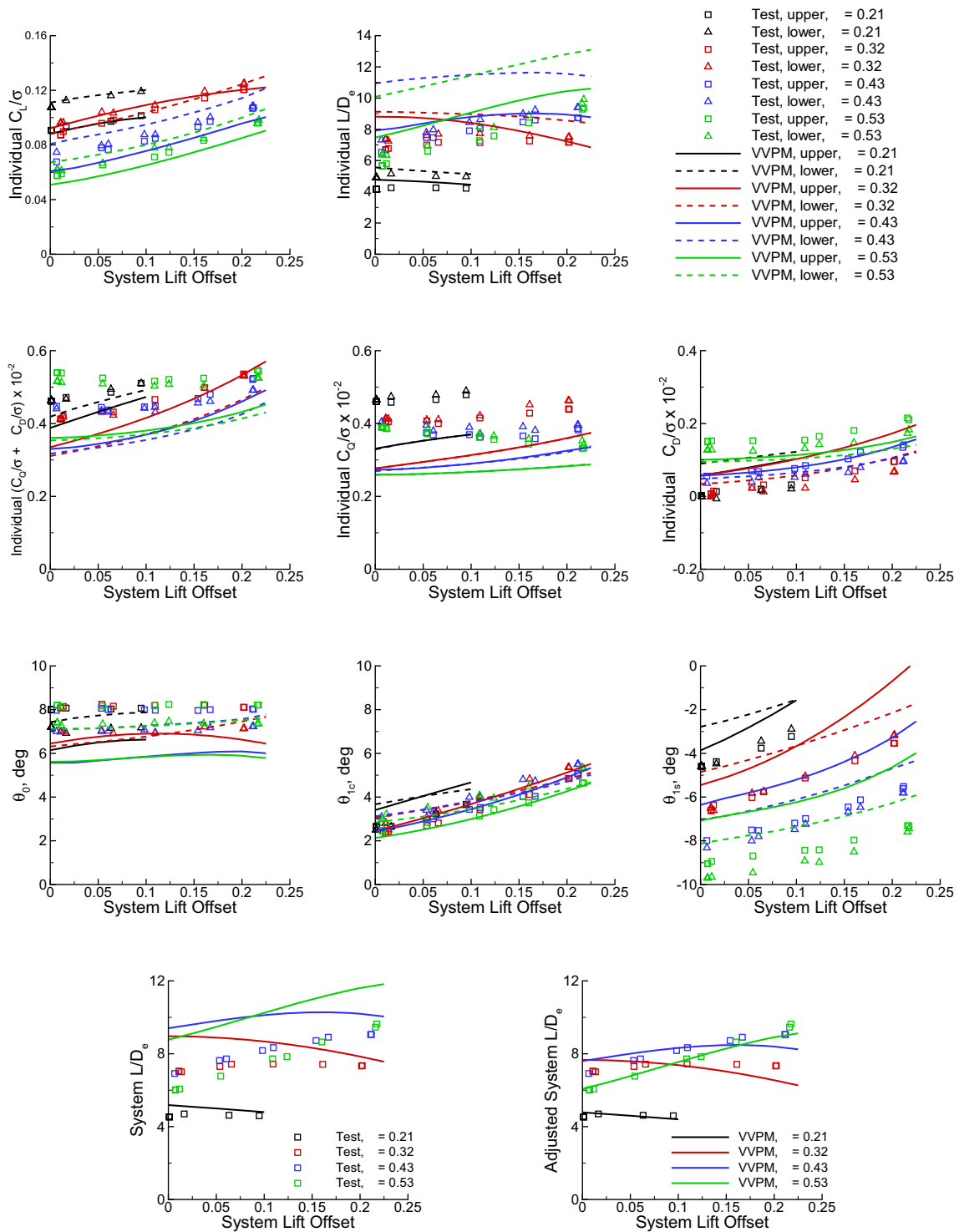
Fig. 10 Rotor parameters as functions of system lift offset in the coaxial rotor configuration for a test upper collective pitch setting of 8° and various advance ratios. Comparison between coupled RCAS–VVPM calculations and test data

but exceptions exist such as the trends in θ_{1s}^L and θ_{1s}^U for the cases of test $\theta_0^U = 8°$ and $\mu = 0.21$.

As it is in the isolated rotor configuration, the benefits of lift offset on system L/D_e also increases with increasing

advance ratio here in the coaxial rotor configuration. Lift offset provides no increase to system L/D_e for $\mu = 0.21$ and only limited increase for $\mu = 0.31$ or 0.32. For $\mu = 0.42$, 0.43,

Table 2 Operating conditions of test points examined for three sweeps

Test point	100815_B_020	100915_B_012	100815_B_003
Lift offset sweep			
μ	0.423	0.426	0.424
System LO	0.002	0.127	0.204
System C_L/σ	0.054	0.050	0.052
ϕ (°)	0	0	0
α_c (°)	0.22	0.20	0.21
Ω, RPM	898	891	897
Test point	100815_E_015	100815_A_005	100815_C_005
Advance ratio sweep			
μ	0.213	0.316	0.527
System LO	0.213	0.207	0.209
System C_L/σ	0.059	0.057	0.053
ϕ (°)	0	0	0
α_c (°)	0.94	0.41	0.14
Ω, RPM	901	893	898
Test point	100815_F_004	100915_F_025	100915_E_028
Rotor-to-rotor phase sweep			
μ	0.316	0.316	0.318
System LO	0.151	0.160	0.164
System C_L/σ	0.088	0.086	0.088
ϕ (°)	0	20	45
α_c (°)	0.63	0.62	0.62
Ω, RPM	897	895	893

and 0.53, system L/D_e increases with lift offset for the entire range examined.

Note that the results here in both the isolated rotor and coaxial rotor configurations are not ideal at evaluating the benefits of lift offset. Ideally, system lift would be kept constant while lift offset is varied. The testing by Cameron and Sirohi [5] was performed by setting the collective pitch of one rotor while adjusting the other pitch angles to achieve certain conditions. However, the system lift was not kept constant with lift offset and was instead increasing with lift offset. This increases the numerator in the L/D_e expressions and thus distorts the L/D_e values in favor of increasing lift offset. Nevertheless, these test data are still useful for the purpose of validating computational aeromechanics tools.

5 Hub Loads and Blade Clearance

This section compares RCAS PVW calculations, RCAS–VVPM calculations, and test data for vibratory (mean removed) rotor hub loads and blade clearance as functions of the upper rotor azimuth in the coaxial rotor configuration.

The hub loads examined are F_Z, M_X, and M_Y in the fixed frame. Unlike in the previous section on rotor performance, the sign convention for M_X^L here is taken as the convention of the upper rotor while sign conventions for F_Z and M_Y are already identical for both rotors. This change in sign convention facilitates an examination of the summed loads of the two rotors. The vibratory hub in-plane loads and torque are not examined since lifting line-based aerodynamics do not calculate the sources (blade section drag and radial drag) of these quantities accurately. The calculated blade clearance is specifically the clearance in the vertical direction between the upper and lower rotor blades at $r = 0.9R$ and is shown as a continuous function, but it is only meaningful at the azimuths of blade crossings.

The test points that are examined here form a "lift offset sweep", an "advance ratio sweep", and a "rotor-to-rotor phase sweep" to isolate the effects of varying LO, μ, and ϕ, respectively, while keeping other rotor parameters approximately constant. Table 2 shows the operating conditions of each of these sweeps. Note that test point 100815_B_003 is listed as part of the lift offset sweep, but it also fits as part of the advance ratio sweep.
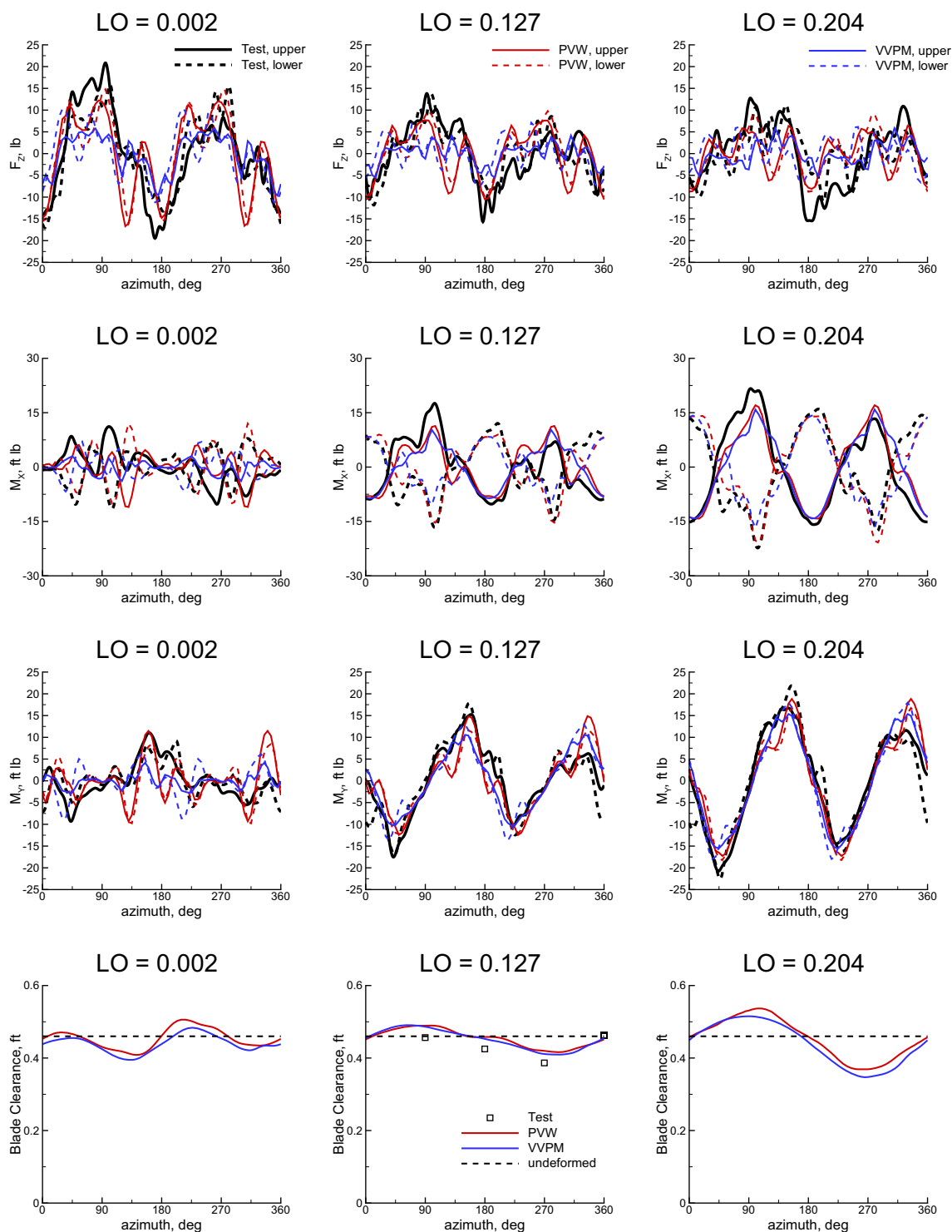
Fig. 11 Vibratory rotor hub loads and blade clearance from a lift offset sweep in the coaxial rotor configuration for $\mu \approx 0.42$

5.1 Lift Offset Sweep

Figure 11 shows the vibratory hub loads and blade clearance for three test points that form a lift offset sweep from $LO = 0.002$ to 0.204. For the near-zero lift-offset case, these two-bladed rotors display a predominantly 2/rev behavior for vertical force while there is no overwhelmingly dominant harmonic for either roll or pitch moment. With increasing lift offset, the trim requirement to satisfy a significant steady roll moment leads to a dominant 2/rev behavior for both roll

and pitch moment that increases in magnitude. Results for the upper and lower rotors are in phase with each other for F_Z and M_Y, but they are 90° out of phase for M_X due to their opposing directions of rotation and these being two-bladed rotors. The trim requirement that both rotors satisfy the same steady roll moment results in the two rotors having nearly identical harmonic magnitudes for M_X and means that the roll moment of the system is nearly balanced even on an instantaneous basis. The test data and both sets of calculations are in agreement in all of these dominant behaviors.

Blade clearance calculations are only meaningful at the blade crossings, which occur for these cases of $\phi = 0$ at azimuths that are multiples of 90°. In each blade clearance plot, a dotted line is drawn and represents the separation between the two rotors in the undeformed state. Measured blade clearance is only available here for the $LO = 0.127$ case. For the nonzero lift-offset cases, blade clearance is minimum at the azimuth of 270°, which is a location where the upper and lower blades are flapping down and up, respectively. The calculations show that this minimum blade clearance decreases with increasing lift offset and test data from other test points confirm this trend. For the case of $LO = 0.127$, the calculations also show the same trends as the test data in how blade clearance varies over a rotor revolution.

5.2 Advance Ratio Sweep

Figure 12, along with the $LO = 0.204$ case from Fig. 11, shows the vibratory hub loads and blade clearance for four test points that form an advance ratio sweep from $\mu = 0.21$ to 0.53. With similar lift offset values of roughly 0.21, the roll and pitch moments all display the dominant 2/rev behaviors stated in the previous subsection. There are not much changes to these 2/rev magnitudes with varying advance ratios. The peak-to-peak magnitudes of the vertical force does increase with increasing advance ratio (as it would for an isolated rotor in this range of advance ratios). Both sets of calculations reflect all of these trends, but they show much lower increases in the peak-to-peak vertical forces with respect to increasing advance ratio than the test data. Measured blade clearance is only available here for the $\mu = 0.21$ case. There are no clear trends to blade clearance with varying advance ratio even if supplemented by data from other test points.

5.3 Rotor-to-Rotor Phase Sweep

With an upper rotor blade positioned at $\psi = 0$ and then following it along its rotational path, rotor-to-rotor phase is defined as the upper rotor azimuth where this blade first crosses a lower blade. It is important to understand how rotor-to-rotor phase changes the summed vibratory loads of the two rotors, because ϕ may be used as a variable to alter the loads that

are transmitted through the shaft to the fuselage on a coaxial rotor helicopter. Figure 13 shows the vibratory hub loads of each individual rotor and the blade clearance for three test points that form a rotor-to-rotor phase sweep from $\phi = 0°$ to 45°. With lift offset values of roughly 0.16, the roll and pitch moments again display dominant 2/rev behaviors. With nonzero ϕ, the results of the lower rotor lead those of the upper rotor by a phase of 2ϕ for F_Z and M_Y. Since the lower rotor shows a phase lag of 90° for M_X compared to the upper rotor for the case of $\phi = 0$, this phase lag reduces to $(90 - 2\phi)$ deg with nonzero ϕ. Both sets of calculations match the test data well for M_X and M_Y due to matching well in the 2/rev harmonic. With increasing ϕ, the RCAS–VVPM calculations show a large increase in the 6/rev harmonic for F_Z that is absent in the test data. Note that this 6/rev issue is not present in either the lift offset or the advance ratio sweep, so it may be an issue that appears for the specific test conditions of the current sweep and is exacerbated by increasing ϕ.

Blade crossings occur at the locations of $\psi = \phi, \phi + 90, \phi + 180$, and $\phi + 270°$. Measured blade clearance is available for the $\phi = 0°$ and 45° cases. The calculations and test data both show that the location of minimum blade clearance is $\psi = 270°$ for $\phi = 0$, but changes to $\psi = 225°$ for $\phi = 45°$.

Figure 14 shows the summed vibratory hub loads of the two rotors for the rotor-to-rotor phase sweep. As stated before for the case of zero ϕ, the summed roll moment is nearly balanced by the two rotors and is merely a small oscillation about zero. With nonzero ϕ, the summed roll moment shows a dominant 2/rev behavior that increases with increasing ϕ. The opposite is true for the summed pitch moment, which shows a dominant 2/rev behavior with nonzero ϕ and decreases with increasing ϕ to the point that it is nearly balanced on an instantaneous basis for $\phi = 45°$. The summed vertical force is dominated by the even-numbered harmonics. Both sets of calculations match the test data well for M_X and M_Y, but not as well for F_Z. As with individual rotor hub loads, the RCAS–VVPM calculations show a large increase in the 6/rev harmonic for F_Z that is absent in the test data.

6 Potential Future Work

This paper is mainly concerned with a qualitative assessment of RCAS at calculating the aeromechanics of lift-offset coaxial rotors. For the most part, both the RCAS PVW and the RCAS–VVPM calculations are successful at calculating the correct trends for rotor performance (especially system L/D_e), blade pitch angles, rotor hub loads (F_Z, M_X, and M_Y), and blade clearance. If closer agreement between the calculations and test data is sought, then two sets of suggestions are offered here as potential future works. One set of suggestions raises awareness of potential issues with the test
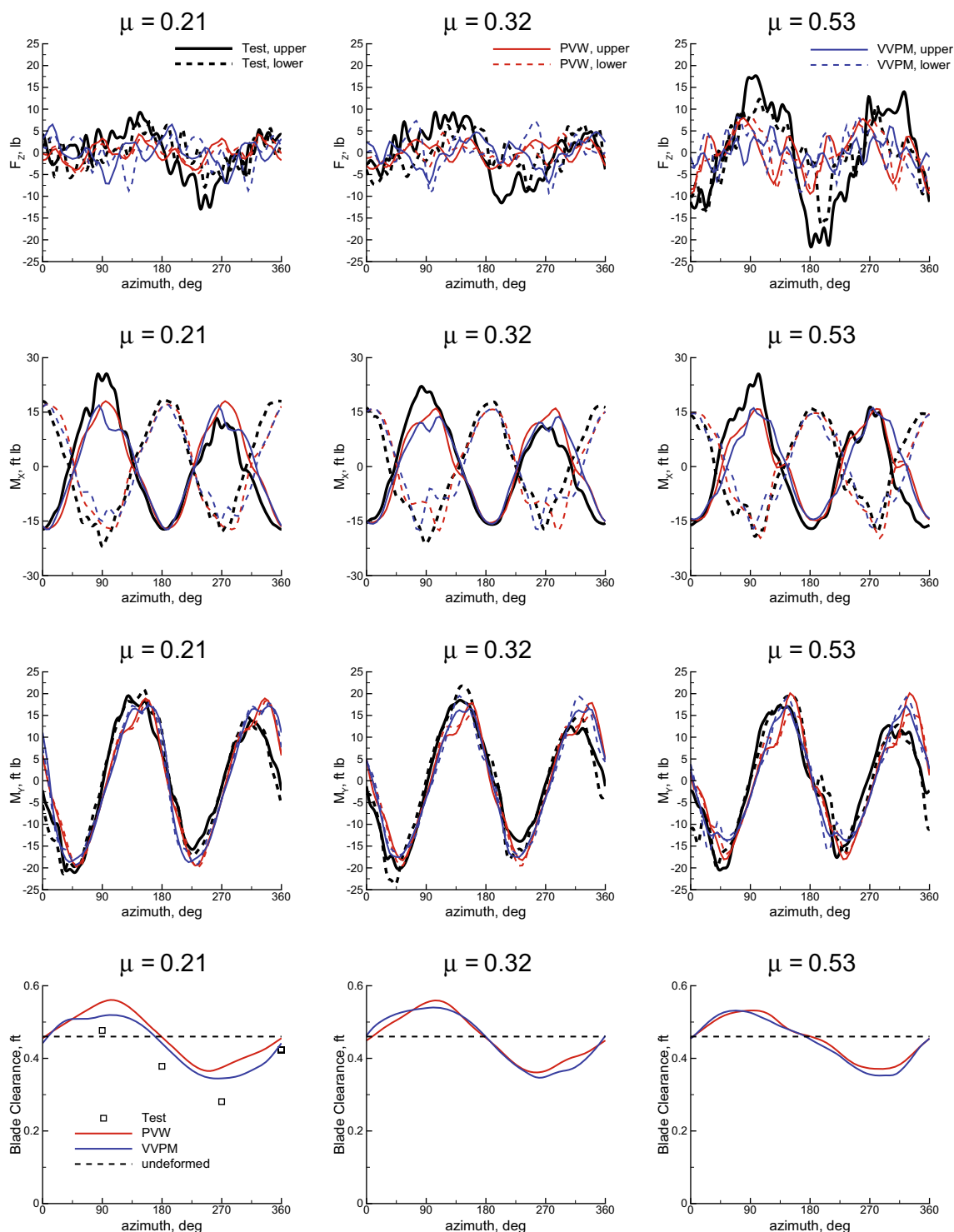
Fig. 12 Vibratory rotor hub loads and blade clearance from an advance ratio sweep in the coaxial rotor configuration for $LO \approx 0.21$

data and another set of suggestions potentially improves the accuracy of the calculations.

The following suggestions are potential issues with the test data that one may want to investigate or at least be aware of:

(1) There are significant differences in the rotor performance parameters between test data measured in the isolated upper and isolated lower rotor configurations.

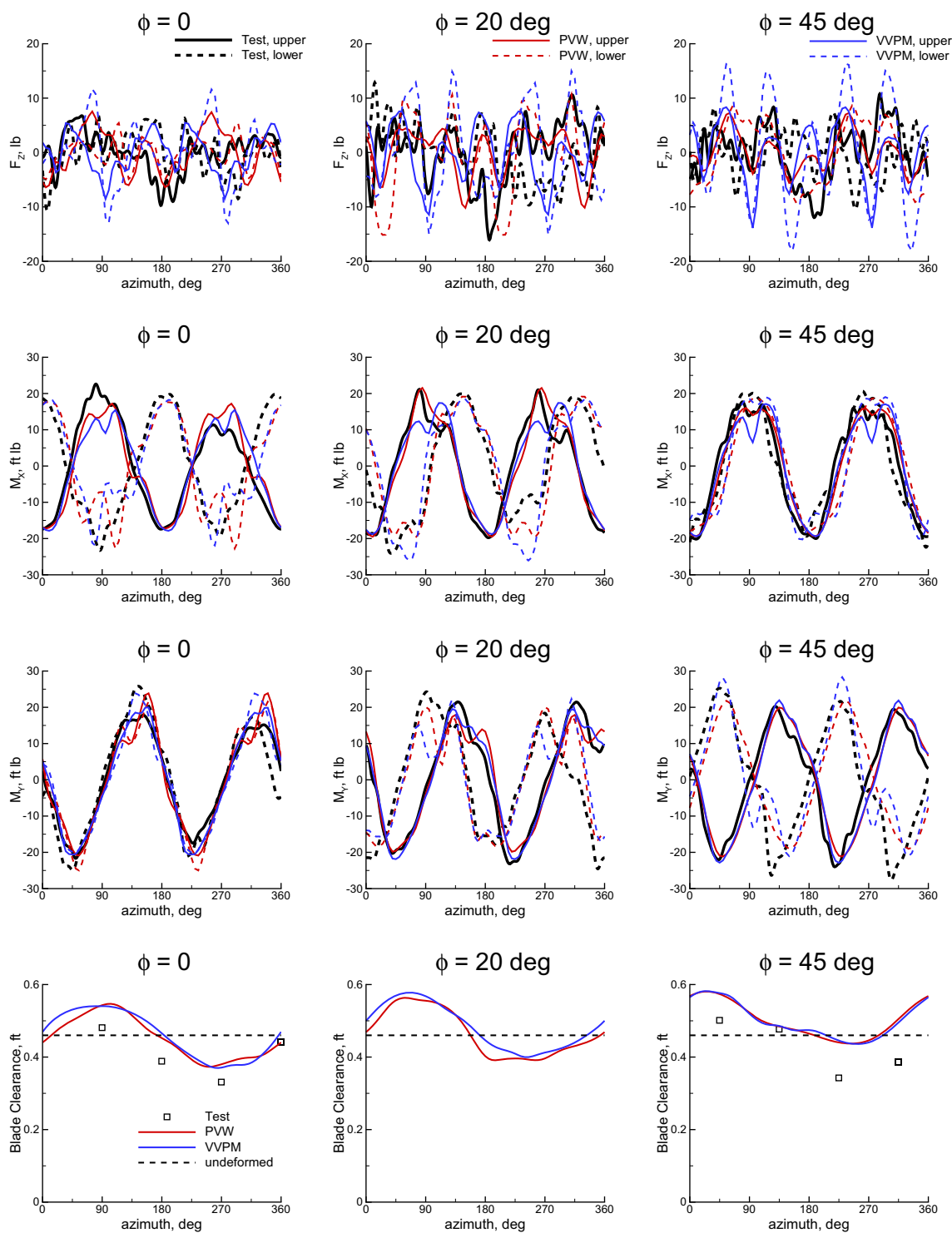(2) As pointed out earlier in the subsection on isolated rotor performance, the measured shaft power displays

Fig. 13 Vibratory rotor hub loads and blade clearance from a rotor-to-rotor phase sweep in the coaxial rotor configuration for $\mu \approx 0.32$ and $LO \approx 0.16$

an unusually high degree of nonlinearity with changes to collective pitch.

The following suggestions may improve the accuracy of the calculations:

(1) Suggestions for improving the accuracy of the elastic multibody dynamics model include modeling the pitch bearing damping, examining the accuracy of the beam properties, and eliminating the isolated rotor approximations. If accurate pitch link force calculations are
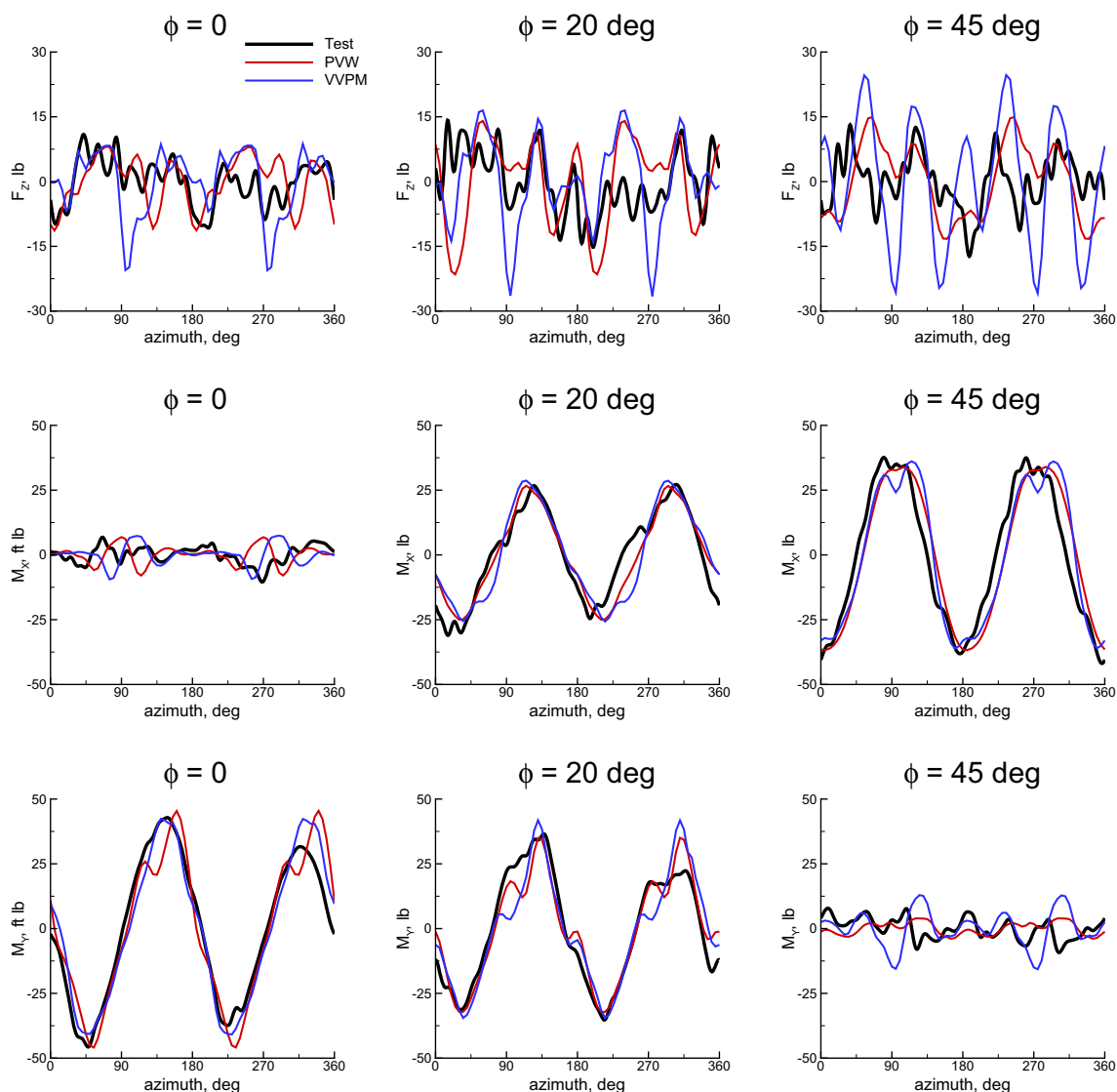
Fig. 14 Summed vibratory rotor hub loads from a rotor-to-rotor phase sweep in the coaxial rotor configuration for $\mu \approx 0.32$ and $LO \approx 0.16$

sought, then pitch bearing damping seems to be a requisite as stated by Schmaus and Chopra [6] as well as Feil et al. [9]. RCAS calculation for non-rotating frequency of the first lag mode from Table 1 is higher than the measured frequency. The beam properties are virtually constant across the blade, except in the inboard region due to the presence of the root reinforcement cuff. The authors did achieve excellent agreement with the measured frequency using an altered beam lag bending stiffness distribution where there is merely a slight increase in the inboard region over the rest of the blade. However, that distribution seems unrealistic given the presence of the root reinforcement cuff. The effects of including the dynamics of the engine, drive train, and test stand are unknown and are potentially important.

(2) Comparisons of vibratory hub loads and blade clearance between calculations and test data for specific test points could be improved by changing the trim target values. The present calculations include $M_X^U = M_X^L = LO\,(R)\left(L^U + L^L\right)/2, M_Y^U = M_Y^L = 0$, and a balanced system torque $(Q^U - Q^L = 0)$ as trim targets, but it would simulate the test conditions more closely using the exact measured values of each of these quantities from each specific test point.

(3) The VR-12 airfoil tables are applied to airloads calculations at the root fairing, but it would be more correct to use airfoil tables that are specifically generated for the shape of the fairing.

7 Conclusions

An elastic multibody dynamics model of a coaxial rotor system with two-bladed hingeless rotors is generated—using the U.S. Army's comprehensive analysis tool RCAS—to provide comparisons of aeromechanics quantities between the RCAS calculations and test data for verifying that RCAS is able to calculate the correct aeromechanics behaviors of lift-offset coaxial rotors. Two different sets of RCAS calculations are presented based on different analyses. One analysis models the aerodynamics of the rotor using a prescribed vortex wake (PVW) inflow model and an airloads model that uses airfoil lookup tables. The other analysis replaces the PVW model of the first with ART Inc's viscous vortex particle method (VVPM) tool for induced velocity calculations and results in a coupled RCAS–VVPM analysis. Prior to showing comparisons in the coaxial rotor configuration, comparisons are first shown in the isolated lower rotor configuration by presenting rotor performance and blade pitch as functions of lift offset for four different advance ratios and for different test collective pitch settings. Next, comparisons are shown in the coaxial rotor configuration by presenting rotor performance and blade pitch as functions of lift offset for four different advance ratios and for two different test upper rotor collective pitch settings. Specific test points—that form a lift offset sweep, an advance ratio sweep, and a rotor-to-rotor phase sweep—in the coaxial rotor configuration are selected for detailed comparisons of rotor hub loads and blade clearance on a time-varying basis. The comparisons lead to the following conclusions:

(1) In the isolated lower rotor configuration, most of the RCAS calculations for rotor performance and blade pitch show the same trends as the test data especially in an aggregate sense. This is less true in a detailed sense such as in the trends of shaft power with collective pitch, which the test data actually show as being unusually nonlinear.

(2) In the coaxial rotor configuration, most of the RCAS calculations for rotor performance and blade pitch again show the same trends as the test data especially in an aggregate sense. This is again less true in a detailed sense such as in the individual lift sharing of the rotors. The RCAS–VVPM calculations generally show closer agreement with test data than the RCAS PVW calculations in lift sharing especially for the test $\theta_0^U = 2°$ cases.

(3) Vibratory individual rotor hub loads for roll and pitch moments show a predominantly 2/rev behavior (from being two-bladed rotors) for nonzero lift-offset cases. The 2/rev harmonic magnitudes of these hub moments increase with increasing lift offset and remain constant with changes to advance ratio. The RCAS calculations are in good agreement with the test data on these trends.

(4) Vibratory individual rotor hub vertical force shows a predominantly 2/rev behavior (again, from being two-bladed rotors) for zero lift offset, but it is not as dominant for nonzero lift offset. As advance ratio increases from 0.21 to 0.53, its peak-to-peak values increase as it would for an isolated rotor. The RCAS calculations correctly capture all of these trends.

(5) From the rotor-to-rotor phase sweep, nonzero ϕ introduces a phase offset of 2ϕ to the vibratory rotor hub loads between the two rotors relative to the zero ϕ case. This profoundly influences the sum of the two rotor hub loads. For the case of $\phi = 0$, the summed roll moment is nearly eliminated on an instantaneous basis while the 2/rev harmonic magnitude is at a maximum for the summed pitch moment. For $\phi = 45°$, the 2/rev harmonic magnitude is at a maximum for the summed roll moment while the summed pitch moment is nearly eliminated on an instantaneous basis. The RCAS calculations correctly capture all of these trends, but the RCAS–VVPM calculations show an excessive amount of 6/rev harmonic content in the hub vertical force that is not present in the test data.

(6) RCAS calculations and test data show the same trends in how blade clearance varies over a rotor revolution. This includes an agreement on the azimuthal location where blade clearance is a minimum.

References

1. Ruddell AJ (1981) Advancing Blade Concept (ABC)^{TM} development test program. AIAA/SETP/SFTE/SAE/ITEA/IEEE 1st Flight Testing Conference. Las Vegas, NV, USA. https://doi.org/10.2514/6.1981-2437

2. Walsh D, Weiner S, Arifian K, Lawrence T, Wilson M, Millott T, Blackwell R (2011) High airspeed testing of the Sikorsky X2 Technology^{TM} Demonstrator. American Helicopter Society 67th Annual Forum. Virginia Beach, VA, USA

3. Lorber PF, Law GK, O'Neil JJ, Matalanis C, Bowles P (2016) Overview of S-97 RAIDER^{TM} Scale Model Tests. In: American Helicopter Society 72nd Annual Forum. West Palm Beach, FL, USA

4. Peterson GL, Saha AB (2016) JMR Development. In: American Helicopter Society 72nd Annual Forum. West Palm Beach, FL, USA

5. Cameron C, Sirohi J (2016) Performance and Loads of a Model Coaxial Rotor Part I: Wind Tunnel Testing. In: American Helicopter Society 72nd Annual Forum. West Palm Beach, FL, USA

6. Schmaus J, Chopra I (2016) Performance and loads of a model coaxial rotor part II: Prediction validations with measurements. In: American Helicopter Society 72nd Annual Forum. West Palm Beach, FL, USA

7. Schmaus J, Chopra I (2016) Validation of predicted vibratory loads of a coaxial rotor at high advance ratios with wind tunnel test data. In: 42nd European Rotorcraft Forum. Lille, France

8. Feil R, Rauleder J, Cameron CG, Sirohi J (2019) Aeromechanics analysis of a high-advance-ratio lift-offset coaxial rotor system. J Aircr 56(1):166–178. https://doi.org/10.2514/1.C034748

9. Feil R, Rauleder J, Hajek M (2017) Vibratory load predictions of a high-advance-ratio coaxial rotor system validated by wind tunnel tests. In: 43rd European Rotorcraft Forum. Milan, Italy

10. Saberi H, Hasbun M, Hong J, Yeo H, Ormiston RA (2015) Overview of RCAS capabilities, validations, and rotorcraft applications. In: American Helicopter Society 71st Annual Forum. Virginia Beach, VA, USA

11. Jain RK, Yeo H, Ho JC, Bhagwat M (2016) An assessment of RCAS performance prediction for conventional and advanced rotor configurations. J Am Helicopter Soc 61(4): Paper 042005. https://doi.org/10.4050/JAHS.61.042005

12. Ho JC, Yeo H (2017) Assessment of comprehensive analysis predictions of helicopter rotor blade loads in forward flight. J Fluids Struct 68:194–223. https://doi.org/10.1016/j.jfluidstructs.2016.09.007

13. Bowen-Davies G, Yeo H (2018) UH-60A rotor performance and loads correlation at high advance ratios. J Aircr 55(1):275–293. https://doi.org/10.2514/1.C034492

14. Ho JC, Yeo H, Bhagwat M (2017) Validation of rotorcraft comprehensive analysis performance predictions for coaxial rotors in hover. J Am Helicopter Soc 62(2): Paper 022005. https://doi.org/10.4050/JAHS.62.022005

15. Singh R, Kang H, Bhagwat M, Cameron C, Sirohi J (2016) Computational and experimental study of coaxial rotor steady and vibratory loads. In: 54th AIAA aerospace sciences meeting. San Diego, CA, USA. https://doi.org/10.2514/6.2016-1787

16. Ho JC, Yeo H (2018) Assessing calculated blade loads of the Tilt Rotor Aeroacoustic Model. J Aircr 55(3):1287–1298. https://doi.org/10.2514/1.C034624

17. Bowen-Davies G (2018) Comparison of vortex wake, VVPM and CFD aeromechanics computations of the Boeing 222 proprotor. In: American Helicopter Society 74th Annual Forum. Phoenix, AZ, USA

18. He C, Zhao J (2009) Modeling rotor wake dynamics with viscous vortex particle method. AIAA J 47(4):902–915. https://doi.org/10.2514/1.36466

19. Zhao J, He C (2010) A viscous vortex particle model for rotor wake and interference analysis. J Am Helicopter Soc 55(1): Paper 012007. https://doi.org/10.4050/JAHS.55.012007

20. Rajmohan N, Zhao J, He C (2014) A coupled vortex particle/CFD methodology for studying coaxial rotor configurations. In: 5th Decennial American Helicopter Society Aeromechanics Specialists' Conference. San Francisco, CA, USA

21. Cameron CG (2016) Comprehensive aeromechanical measurements of a model-scale, coaxial, counter-rotating rotor system. Ph.D. Dissertation, University of Texas at Austin, Austin, TX, USA

22. Hodges DH, Dowell EH (1974) Nonlinear equations of motion for the elastic bending and torsion of twisted nonuniform rotor blades. NASA TN D-7818

23. Langer H, Peterson RL, Maier TH (1996) An experimental evaluation of wind tunnel wall correction methods for helicopter performance. In: American Helicopter Society 52nd Annual Forum. Washington, DC, USA

24. Barlow JB, Rae WH, Jr., Pope A (1999) Low-speed wind tunnel testing, 3rd edn. Wiley, New York

25. Yeo H, Truong K, Ormiston RA (2014) Comparison of one-dimensional and three-dimensional structural dynamics modeling of advanced geometry blades. J Aircr 51(1):226–235. https://doi.org/10.2514/1.C032304

26. Srinivasan GR, Baeder JD (1993) TURNS: a free-wake Euler/Navier–Stokes numerical method for helicopter rotors. AIAA J 31(5):959–962. https://doi.org/10.2514/3.49036

27. Theodorsen T (1935) General theory of aerodynamic instability and the mechanism of flutter. NACA Rep 496

28. Greenberg JM (1947) Airfoil in sinusoidal motion in a pulsating stream. NACA TN 1326

29. Wachspress DA, Yu K, Saberi H, Hasbun MJ, Ho JC, Yeo H (2012) Helicopter rotor airload predictions with a comprehensive rotorcraft analysis. American Helicopter Society 68th Annual Forum. Fort Worth, TX, USA

30. Yu K, Wachspress DA, Saberi H, Hasbun MJ, Ho JC, Yeo H (2012) Helicopter rotor structural load predictions with a comprehensive rotorcraft analysis. In: American Helicopter Society 68th Annual Forum. Fort Worth, TX, USA